Chemistry & Biology
Resource

Spatiotemporal Control of Fibroblast Growth Factor Receptor Signals by Blue Light

Nury Kim,[1,5] Jin Man Kim,[3,5] Minji Lee,[2] Cha Yeon Kim,[4] Ki-Young Chang,[1] and Won Do Heo[1,2,*]
[1]Center for Cognition and Sociality, Institute for Basic Science (IBS), Daejeon 305-701, Republic of Korea
[2]Department of Biological Sciences, Korea Advanced Institute of Science and Technology (KAIST), Daejeon 305-701, Republic of Korea
[3]Graduate School of Medical Science and Engineering, Korea Advanced Institute of Science and Technology (KAIST), Daejeon 305-701, Republic of Korea
[4]Graduate School of Nanoscience and Technology, Korea Advanced Institute of Science and Technology (KAIST), Daejeon 305-701, Republic of Korea
[5]Co-first author
*Correspondence: wondo@kaist.ac.kr
http://dx.doi.org/10.1016/j.chembiol.2014.05.013

SUMMARY

Fibroblast growth factor receptors (FGFRs) regulate diverse cellular behaviors that should be exquisitely controlled in space and time. We engineered an optically controlled FGFR (optoFGFR1) by exploiting cryptochrome 2, which homointeracts upon blue light irradiation. OptoFGFR1 can rapidly and reversibly control intracellular FGFR1 signaling within seconds by illumination with blue light. At the subcellular level, localized activation of optoFGFR1 induced cytoskeletal reorganization. Utilizing the high spatiotemporal precision of optoFGFR1, we efficiently controlled cell polarity and induced directed cell migration. OptoFGFR1 provides an effective means to precisely control FGFR signaling and is an important optogenetic tool that can be used to study diverse biological processes both in vitro and in vivo.

INTRODUCTION

Fibroblast growth factor receptors (FGFRs) are highly conserved receptor tyrosine kinases that bind to fibroblast growth factors (FGFs). The FGF family is the largest group of growth factors, with 22 members and 7 groups in humans (Itoh and Ornitz, 2004), and they regulate diverse biological events, including development, wound healing, and angiogenesis (Klint and Claesson-Welsh, 1999). Upon binding with FGFs, FGFRs dimerize and *trans*-autophosphorylate multiple tyrosine residues, thereby providing docking sites for downstream components such as phosphatidylinositol 3-kinase (PI3K), mitogen-activated protein kinase (MAPK), and phospholipase C (PLC) (Mohammadi et al., 1996).

The FGFR-FGF interactions have complex properties because of the promiscuous binding of FGF to the different FGFR isoforms (Turner and Grose, 2010). Moreover, the activities of FGFRs are intricately controlled by distinct interactions with FGFs and cofactors in a defined space and time (Powers et al., 2000). Given these properties of FGFR, promiscuous binding and spatiotemporal regulation, it is difficult to delineate the specific role of each isoform in a certain biological context, which gives rise to the need for a tool capable of specifically and precisely regulating the FGFR system. To date, many approaches have been introduced to study FGFR signaling pathways. Despite extensive use in previous research, recombinant peptides of FGF ligands exhibit complex effects because of their redundant binding to FGFR isoforms. Genetic perturbation studies, represented by overexpression and knockout strategies, have tried to elucidate the specific function of FGF-FGFR systems. However, these methods have practical difficulties, such as delayed responses and constitutive alterations in gene expression (Stockwell, 2000).

The chemically induced dimerization (CID) system is one alternative for compensating for those drawbacks. The genetically engineered CID system is based on a concept in which the proximity between target proteins can be increased through the engineered docking site by a pharmacological dimerizer (Neff and Blau, 2001). This method has proven to be useful for elucidating the roles of specific types of receptors in various biological events. For example, chimeric FGFR subtypes fused with mutated FK506 binding protein showed the distinct effects of individual receptors on the progression of breast and prostate cancer (Freeman et al., 2003; Xian et al., 2005). However, these tools also have limitations that are common with chemically based approaches, such as potential side effects from the addition of exogenous small molecules, low reversibility, a prolonged diffusion time of substances, and low spatial precision.

Optogenetic approaches, which have been developed and expanded rapidly in application over the last few years, have been suggested as powerful means to overcome these limitations. Meanwhile, various photo-inducible proteins have been introduced to regulate protein interaction by light stimulation (Levskaya et al., 2009; Wu et al., 2009). One is the photolyase homology region from the photosensory protein cryptochrome 2 (CRY2PHR) of *Arabidopsis thaliana*. This protein undergoes a conformational change and promotes homointeraction upon blue light illumination (Yu et al., 2009). CRY2PHR is an enticing optogenetic module for use in optogenetic studies of intracellular signaling in mammalian systems (Bugaj et al., 2013) because of its fast responsiveness with subsecond time resolution, subcellular spatial resolution, and no need for exogenous cofactors (Kennedy et al., 2010).

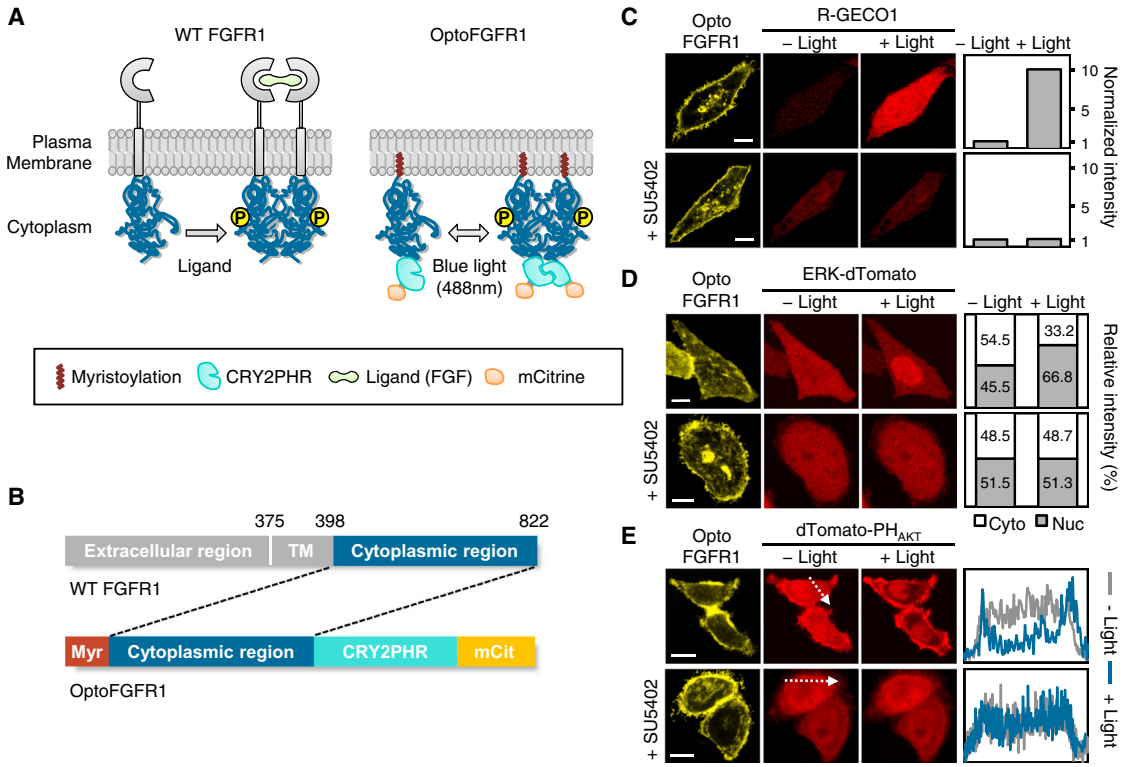

Figure 1. Generation and Characterization of OptoFGFR1

(A) Schematic representation of wild-type (WT) FGFR1 and optoFGFR1.

(B) Design of the optoFGFR1 construct. The cytoplasmic region of FGFR1 (amino acids 398–822) was inserted between the myristoylation signal peptide (Myr) and CRY2PHR. TM, transmembrane region; mCit, mCitrine.

(C–E) Fluorescence images of HeLa cells expressing optoFGFR1 (yellow) and biosensors (red) for (C) the PLCγ pathway, R-GECO1; (D) the ERK pathway, ERK-dTomato; and (E) the PI3K pathway, dTomato-PH_{AKT}. The cells were illuminated by continuous blue light (488 nm, 7 μW) with or without treatment of an FGFR-specific kinase inhibitor (SU5402). The quantified results in the right panel of each image show the normalized cytoplasmic intensity of R-GECO1, the relative intensity of the cytoplasm (cyto, empty bar), and the nucleus (nuc, gray bar) of ERK-dTomato and line intensity histograms of dTomato-PH_{AKT} fluorescence intensity across the white dotted arrows in gray (before light stimulation) and blue (after light stimulation).

Scale bars, 10 μm. See also Figures S1 and S2.

In this study, we developed a light-inducible chimeric receptor, called optoFGFR1, by utilizing CRY2PHR as a regulatory component and attaching it to the cytoplasmic region of FGFR1 under the rationale that the homointeraction property of CRY2PHR is sufficient to activate FGFR1. Through this technology, we present the spatiotemporal regulation of the FGFR signal and also highlight the role of optoFGFR1 in regulating membrane protrusion and the direction of migrating cells.

RESULTS

Generation of Light-Inducible FGFR1

We designed a light-inducible module for activating FGFR signals by use of the light-dependent homointeractive domain PHR from cryptochrome 2 (CRY2PHR). In particular, we hypothesized that light-inducible homointeraction of CRY2PHR would bring FGFR1s into close proximity, leading to activation of the receptor even in the absence of its ligand (Figure 1A). This optogenetic module, optoFGFR1, consists of CRY2PHR (amino acids 1–498) (Kennedy et al., 2010), the cytoplasmic region of human FGFR1 (amino acids 398–822), and a myristoylation signal peptide (Figure 1B).

Light-Induced Activation of FGFR1 Signaling Pathways by OptoFGFR1

We initially performed time-lapse live cell imaging to examine the functionality of optoFGFR1 by confirming that light activates the canonical FGFR pathways. To activate optoFGFR1 via light-induced CRY2PHR homointeraction, blue light (488 nm, 7 μW) was illuminated onto HeLa cells coexpressing optoFGFR1 and each optical biosensor for distinct FGFR canonical pathways: R-GECO1 (Zhao et al., 2011), ERK-dTomato, and dTomato-PH_{AKT}, reflecting the PLCγ, MAPK, and PI3K pathways, respectively. After illumination, ERK-dTomato and dTomato-PH_{AKT} were translocated into the nucleus and on the plasma membrane, respectively, and the fluorescence intensity of R-GECO1 was increased in optoFGFR1-expressing cells (Figures 1C–1E). Under the same conditions, there was no change in these signals after treatment with SU5402, a FGFR-specific tyrosine kinase inhibitor (Figures 1C–1E, bottom panel). For verification of signal specificity, we constructed two optoFGFR1 mutants: a PLCγ binding mutant of optoFGFR1 (Y766F) (Mohammadi et al., 1991) and CRY2PHR-deleted optoFGFR1 (ΔCRY2PHR). The Y766F and ΔCRY2PHR mutants could not elevate the R-GECO1 signal regardless of light illumination,

implying that CRY2PHR-dependent homointeraction of cytoplasmic FGFR1 is sufficient for activation of FGFR signaling (Figure S1A available online). We also evaluated the functionality of optoFGFR1 by comparing the phosphorylation of ERK in optoFGFR1-expressing HeLa cells that were illuminated for 5 or 15 min with nontransfected HeLa cells treated with bFGF (10 ng/ml) for 5 or 15 min. Compared with the basal state, there were remarkable increases in the phosphorylation of ERK1/2 that were sustained in all time periods in the bFGF-treated cells and the illuminated cells (Figure S1B). These results suggest that three major pathways of FGFR could be readily and specifically activated through optoFGFR1 upon light exposure.

An increase of proximity between receptors upon dimerization is the key process in the activation of receptor tyrosine kinases (Hubbard and Till, 2000). To visualize the increase of proximity between optoFGFR1 upon light illumination, we conducted a fluorescence resonance energy transfer (FRET) assay in cells coexpressing mCitrine- and mCerulean-tagged optoFGFR1 (Figure S1C). Upon light illumination, we not only observed a significant increase in FRET signal after light illumination (Figure S1D; $p < 0.001$) but also observed clustering of optoFGFR1 on the basal cell membrane through total internal reflection fluorescence (TIRF) microscopy (Figure S1F). These results provide direct evidence of the homointeraction property of optoFGFR1 upon light illumination. Notably, these results could not be observed with optoFGFR1 containing a light-insensitive CRY2PHR mutant, CRY2PHR(D387A) (Liu et al., 2008) (Figures S1D and S1F), implying that homointeraction of optoFGFR1 is mainly induced by CRY2PHR.

Under physiologically relevant conditions, activation of FGFR via ligands leads to receptor internalization and ubiquitination (Wong et al., 2002) and to signaling alterations because of changed localization (Wiley and Burke, 2001). Therefore, we investigated whether light-induced activation of optoFGFR1 undergoes the same internalization process. In particular, we compared the localization patterns of optoFGFR1 with those of the Rab5b small GTPase, which is involved in the trafficking of the FGFR signaling complex (Sandilands et al., 2007), at certain time periods (0, 20, and 40 min) after light illumination. Within 20 min after illumination, optoFGFR1 formed small puncta and colocalized into early endosomes marked by mRFP-Rab5b. Over time, those complexes accumulated adjacent to the nucleus (Figures S2A and S2C). However, optoFGFR1 without the cytoplasmic FGFR1 region (ΔFGFR1) was not colocalized with Rab5B and did not show any punctum formation and translocation despite light stimulation. These results indicate that optoFGFR1 can be internalized following light stimulation and that this process is mainly dependent on the activated cytoplasmic FGFR1 region (Figures S2B and S2D).

Taken together, our light-responsive chimeric protein, optoFGFR1, is not only efficient and specific in inducing the activation of FGFR signaling by light illumination but also biologically relevant to the wild-type FGFR1.

Spatiotemporal Regulation of FGFR Signaling pathways by Illumination

The ability to precisely control cellular functions with high spatial and temporal resolution is one of the main advantages

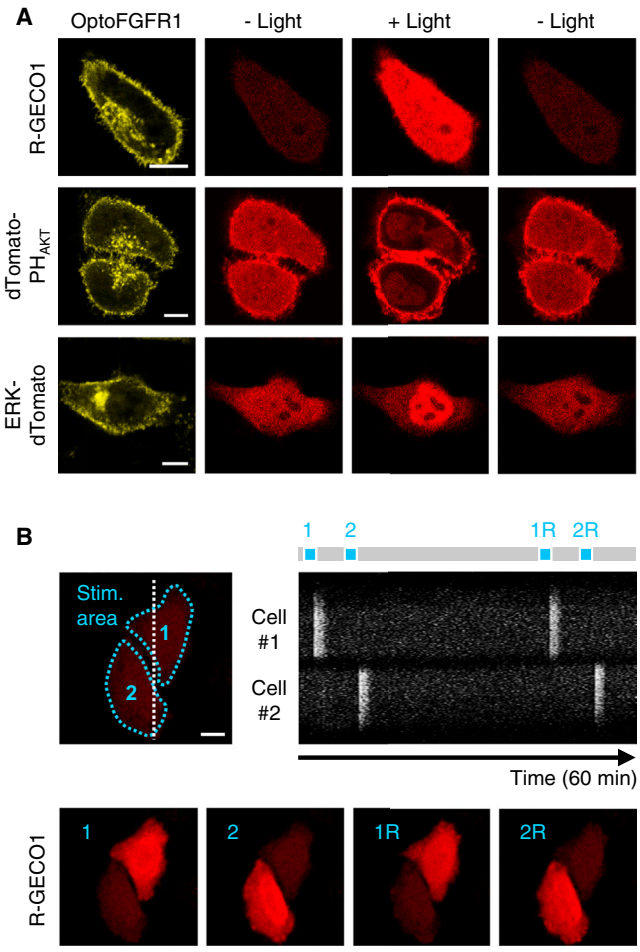

Figure 2. Spatiotemporal Control of FGFR1 Downstream Signals by Light

(A) Changes in three downstream pathways of optoFGFR1 expressing HeLa cells after a single pulse of light (488 nm, 7 μW).

(B) Reversible and individual activation of PLCγ signals in HeLa cells expessing optoFGFR1. Cells were sequentially and repeatedly illuminated with blue light (488 nm, 1 μW) as illustrated in the upper left panel and upper right gray bar (blue square, time of illumination). Kymograph of R-GECO1 intensity drawn along the dashed white line is in the upper right panel. Lower panel images show maximal R-GECO1 responses of each cell after activation. Stim. area, stimulated area; R, repeated stimulation.

Scale bars, 10 μm. See also Figures S3 and S4 and Movie S1.

of optogenetics. Therefore, we characterized optoFGFR1 based on the high spatiotemporal resolution of light exposure, reversibility of the system, and versatility of the intracellular signaling. First of all, we assessed the temporal resolution of optoFGFR1. HeLa cells coexpressing optoFGFR1 and each biosensor for one of three canonical pathways were stimulated with a single pulse of blue light (0.5 s), and signal changes were monitored simultaneously. Under brief light exposure, all three pathways, PLCγ, PI3K, and MAPK, were transiently activated in minutes (Figure 2A). Next, we evaluated the spatial precision and reversibility of optoFGFR1. We utilized R-GECO1 as an indicator to clearly visualize the on/off transition of PLCγ signaling in two adjacently located cells. Blue light was given sequentially to each cell, and each cell in the region of

illumination responded immediately. The level of calcium increased repeatedly in a similar manner during the second cycle of illumination (Figure 2B; Movie S1).

To evaluate the responsiveness of optoFGFR1, the activation kinetics of light-mediated FGFR1 signaling were compared with those of the existing, chemically induced approach. We constructed additional FGFR signaling activator protein, inducible human FGFR (ihFGFR1), which can be activated by treatment with a chemical dimerizer, AP20187 (Welm et al., 2002) (Figure S3A). After treatment with AP20187 or continuous illumination, we quantified the change of fluorescence intensity over time for each biosensor of canonical pathways and calculated the half-maximal time for activation ($Ta_{1/2}$, see Experimental Procedures). The activation kinetics of canonical signaling pathways by ihFGFR1 were significantly slower than those of optoFGFR1 ($p < 0.005$; Figures S3B–S3E), probably because of the time required for diffusion. The rapid change of signaling pathways clearly demonstrates the fast response of optoFGFR1.

Moreover, we found that signaling kinetics were affected by the expression level of optoFGFR1 and light intensity, although the magnitude of activation was not affected. The activation kinetics of PLCγ signaling became faster as the light intensity or expression level of optoFGFR1 increased (Figure S4). We also observed that the deactivation kinetics were faster in cells with fast activation kinetics, implying a possible negative feedback mechanism in the signaling pathway (Taylor, 1998).

Versatile Control of Signaling Dynamics by Modulation of Illumination

Transient versus sustained activation of signaling pathway has been regarded as the determinant of signaling specificity, especially in the ERK pathway (Marshall, 1995). Therefore, we monitored the change of ERK signaling kinetics according to the frequency or duty cycle of photostimulation in HeLa cells expressing optoFGFR1. Various ERK translocation patterns were observed in response to photostimulation with 10- to 60-min intervals. The minimal interval of time, 10 min, was determined by the results from a previous report on dissociation kinetics of CRY2PHR clusters (decay constant, 5.4 ± 0.4 min) (Bugaj et al., 2013). At the highest frequency, 10 min, repeated stimulation of optoFGFR1 elicited an accumulation of ERK in the nucleus for longer than 2 hr, and the sustained level was similar to that seen with bFGF treatment (Figure 3A, upper panels). With lower frequencies (30- and 60 min intervals), ERK kinetics showed transient and pulsatile patterns, and the cyclic period corresponded with its interstimulus interval (Figure 3A, lower panels).

To investigate the effect of the duty cycle, we applied blue light with various durations within a period of 20 min (1%–50% duty cycles). Interestingly, the major factor of ERK signals affected by varying duty cycles was not kinetics but the magnitude of activity. Nuclear ERK intensity was increased 4-fold as the duty cycle increased up to 50% (Figure 3B). This increasing pattern upon continuous illumination seems to result from the characteristics of CRY2PHR because a similar pattern was observed in a previous report (Bugaj et al., 2013). Taken together, these observations demonstrate that optoFGFR1 can distinctly regulate signaling pathways depending on the frequency and duration of light stimulation.

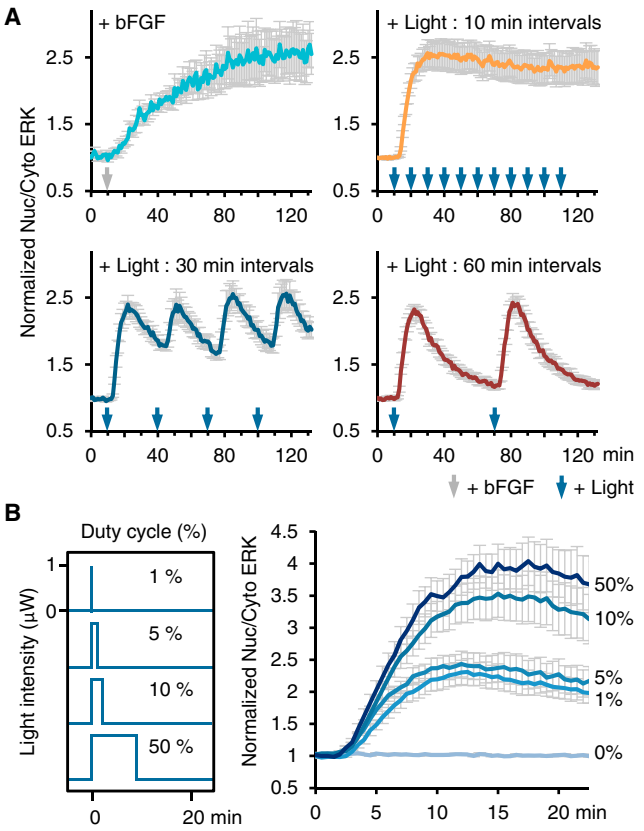

Figure 3. Fine-Tuned FGFR1 Signaling Activity through Diverse Light Inputs

(A) The change of ERK signaling kinetics according to the frequency of photostimulation. HeLa cells coexpressing optoFGFR1 and ERK-dTomato were either treated with bFGF (10 ng/ml) or illuminated repeatedly (488 nm, 7 μW) at 10-, 30-, and 60-min intervals ($n > 6$). Gray and blue arrows represent time points of bFGF treatment and light illumination, respectively. nuc, nucleus; cyto, cytoplasm.

(B) The effect of the duty cycle of photostimulation on the magnitude of ERK translocation in HeLa cells. Blue light was applied for 0, 0.2, 1, 2, and 10 min, which corresponds to 0%, 1%, 5%, 10%, and 50% of duty cycles (percentage of illumination duration/total period; see Experimental Procedures). The graph in the right panel shows the change of ERK translocation over a time period of 20 min.

Error bars indicate SEM.

Regulation of Cell Polarity through optoFGFR1

Next, we identified the effect of optoFGFR1 on specific cell functions in which multiple signal pathways are orchestrated. FGF is one of several crucial factors in angiogenesis, especially in the actin-based motility of endothelial cells (Lamalice et al., 2007). Moreover, it is well known that endothelial cells, regardless of their origin, mainly express FGFR1 (Bastaki et al., 1997). We reasoned that precise activation of FGFR1 through optoFGFR1 could dissect complex signaling pathways involved in cell migration and reveal the specific role of FGFR1 in this response. Accordingly, we selected human umbilical vein endothelial cells (HUVECs) that were transfected with mCherry-Lifeact (Riedl et al., 2008) and optoFGFR1 as a model system for visualizing cytoskeletal changes related to cell motility upon optoFGFR1 activation. After serum starvation, transfected HUVECs

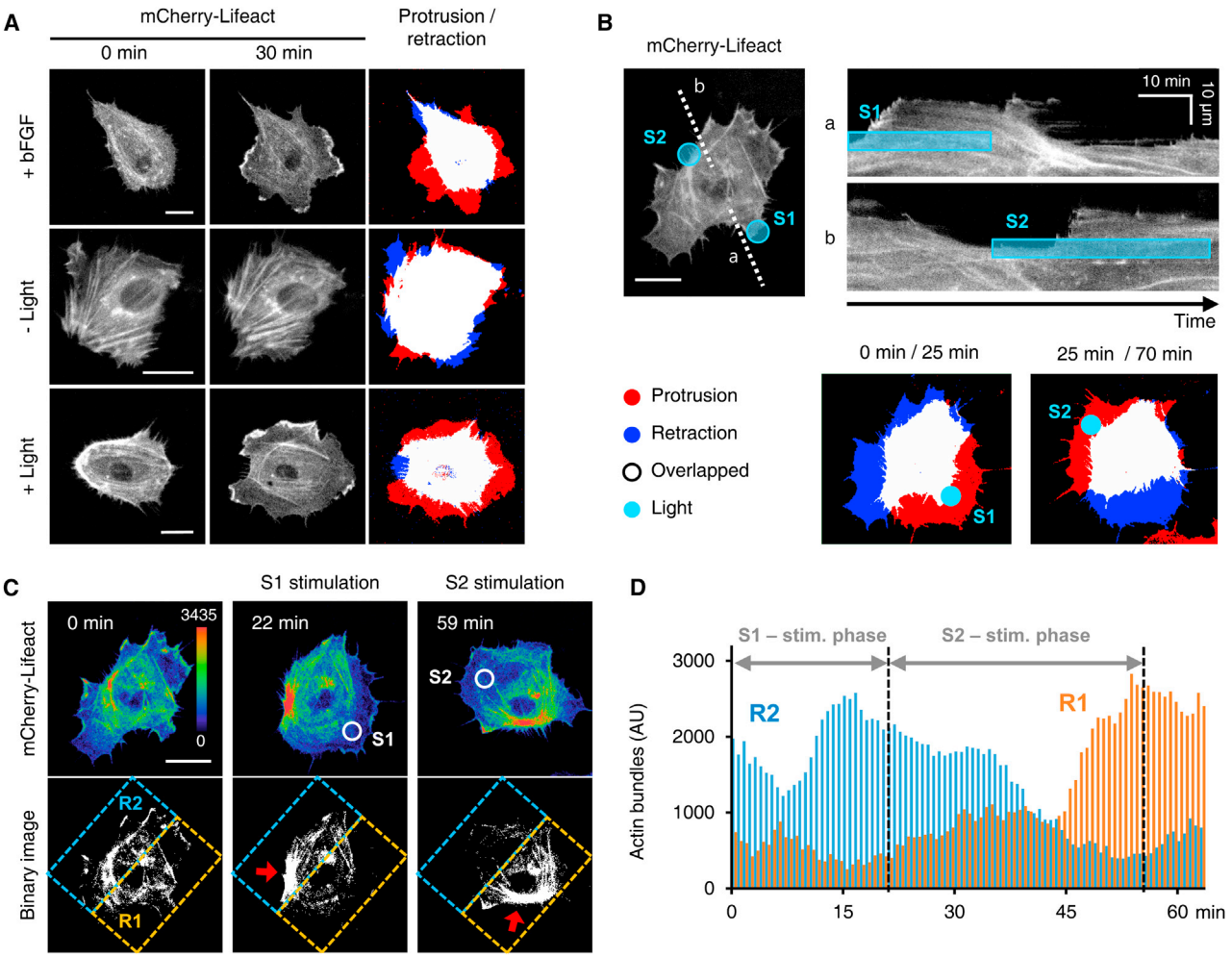

Figure 4. Light-Induced Membrane Protrusion and Cell Polarization

(A) Morphological changes of HUVECs coexpressing optoFGFR1 and mCherry-Lifeact that were treated with bFGF (100 ng/ml) (+ bFGF), unilluminated (– Light), or illuminated with blue light (488 nm, 7 μW, and 30 s intervals) (+ Light). The right panel shows protrusions and retractions at 0 and 30 min (red, protrusion; blue, retraction; white, overlapping area).

(B) Polarity change upon partial stimulation by light. Repeated partial stimulation (488 nm, 1 μW, and 30 s intervals) was applied to the peripheral region of a HUVEC. Two different sites (light blue region, S1 or S2) were illuminated sequentially, and adjacent linear regions (white dotted line, a and b) were drawn by the kymograph (upper right panel). The light-induced change in cell morphology is presented as a protrusion/retraction graph in the lower panel (red, protrusion; blue, retraction; white, overlapping area; light blue, illuminated point).

(C) Changes in stress fiber distribution during partial light stimulation in Figure 4B. mCherry-Lifeact images are illustrated by a pseudocolored intensity image that focused on actin filaments (upper panel). This image clearly shows concentrated actin filaments at opposite sides of the illuminated area (red arrow) and that the whole cell region is divided into two distinct parts (yellow and blue dotted squares, R1 and R2), with separate quantification of the amounts of actin bundles in each part.

(D) Quantified amount of actin bundles in two distinct regions (R1 and R2) during the S1 and S2 stimulation (stim.) phases. AU, arbitrary unit.

Scale bars, 20 μm. See also Movie S2.

presented spontaneous and intermittent protrusion-retraction cycles covering the entire cell boundary (Tkachenko et al., 2011). Upon either bFGF (100 ng/ml) treatment or repeated illumination (30 s intervals) of the whole cell area, global lamellipodia were induced around the entire cell edge (Figure 4A), demonstrating a general effect of FGFR1 activation on actin remodeling in a physiological context.

We next examined the effect of local delivery of light in HUVECs coexpressing optoFGFR1 and mCherry-Lifeact. Repeated blue light illumination of a small area of the cell periphery (S1, 5 μm radius) induced lamellipodia that were localized around the region of illumination (Figure 4B). Interestingly, there was a simultaneous retraction of the membrane in the region opposite the illumination spot (Figure 4B, protrusion/retraction map; Movie S2), suggesting that asymmetric activation of FGFR1 in a single cell establishes cell polarity. When the illumination spot was shifted to a different region of the same cell, the polarity was changed according to the position of light exposure (Figure 4B). Moreover, we could visualize the dynamic assembly and disassembly of thick actin fibers at the opposite

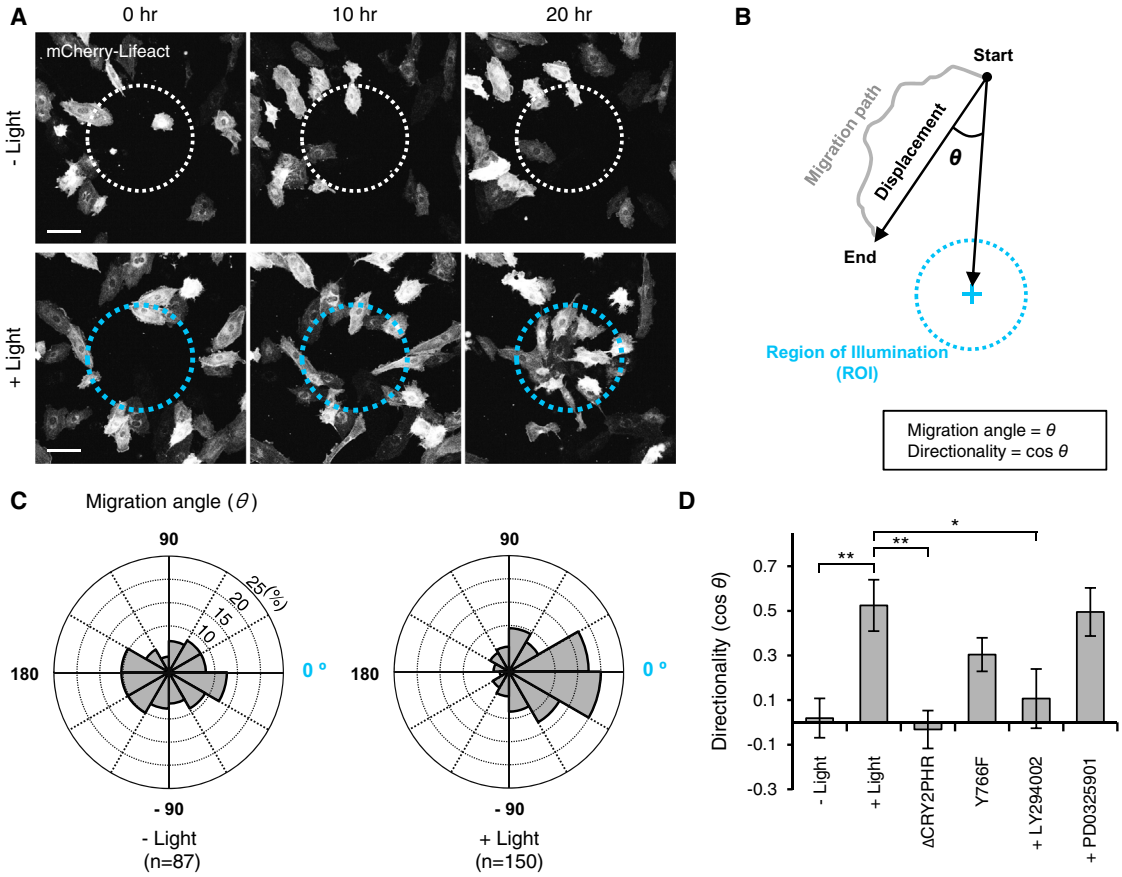

Figure 5. Light-Induced Directed Cell Migration and Related Signaling Pathways

(A) OptoFGFR1-mediated phototaxis model. Circular blue light (160 μm radius, blue dotted circle) was applied to the center of the imaging field (488 nm, 30 μW, and 30 s intervals) in which HUVECs expressing optoFGFR1 and mCherry-Lifeact were sparsely plated and serum-starved (6 hr). Cell movement was monitored for 20 hr and compared with the group without light illumination (white dotted circle).

(B) Schematic illustrating the methods used to determine migration angle (θ) and directionality (cos θ).

(C) Distribution of migration angles in a group of cells with and without light stimulation. Cells were classified by migration angle, measured as the angle between cell displacement and the center of the light, as in Figure 5B. The percentage of the cells that were kept in darkness (– Light, n = 87) and illuminated (+ Light, n = 150) is plotted in an angular histogram.

(D) Comparison of the directionality (cos θ) of optoFGFR1-expressing HUVECs with inhibition of three different pathways (n > 30 in all groups). Cells were illuminated with blue light on the circular region. The FGFR signaling pathways were inhibited using a CRY2PHR deletion (ΔCRY2PHR), Y766F mutation, 50 μM LY294002, and 50 nM PD0325901. A directionality value near 1 indicates that cells moved toward to the center of the light. Asterisks indicate significant differences (*$p < 0.05$, **$p < 0.005$). Error bars indicate SEM.

Scale bars, 100 μm. See also Figure S5 and Movies S3 and S4.

side of the illuminated region and in the area of light exposure, respectively (Figure 4C). A quantified amount of actin bundles in two distinct regions (the region of light stimulation and the opposite side) also clearly indicates that the distribution of actin bundles was largely dependent on the region of illumination (Figure 4D). This asymmetric distribution of actin fibers provides important evidence for protrusive and retractile dynamics in different regions of a cell induced by optoFGFR1. In short, we confirmed that light-induced global or local activation of optoFGFR1 induces the dynamic changes in the actin cytoskeleton represented by formation of lamellipodia and stress fibers, and reorganization of cell polarity. With these results, we strongly emphasize that optoFGFR1 facilitates the fine-tuned and precise spatial activation of FGFR1 on a subcellular level.

Light-Induced Directed Cell Migration by OptoFGFR1

We hypothesized that protrusive and polarized morphological changes induced by optoFGFR1 suggest the possibility that directed cell migration can be induced through local illumination. To confirm this conjecture, we designed a "phototaxis model" in which optoFGFR1-expressing cells are guided into a circular field of blue light (160-μm radius) (Figure 5A). HUVECs cotransfected with optoFGFR1 and mCherry-Lifeact were sparsely plated and subjected to serum starvation before tracking their movement based on the center of the nucleus. Interestingly, the cells consistently migrated toward the illuminated area (Figure 5A; Movie S3) for 20 hr, whereas the cells in a field without light exposure moved in random directions (Figure 5A; Movie S4). Notably, prolonged light stimulation did not have an adverse effect on cell viability (Figures S1G and S1H). We sought to

quantify the cell movement by measuring the migration angle (θ), defined as the angle between two paths regarding either displacement of each cell or the segment connecting the start point of the cell to the center of the illuminated region (Figure 5B). An angular histogram, which depicts the distribution of migration angles, clearly demonstrates the tendency of cells to migrate toward the illuminated region (Figure 5C), indicating that FGFR1 signaling can determine the directionality of migrating cells.

Three major signaling pathways of FGFR1, MAPK, PLCγ, and PI3K, are known to be related to directionality in various cell types (Shi et al., 2011; Tsai et al., 2014; Welf et al., 2012). With the optoFGFR1-mediated phototaxis model, we investigated the contributions of these signaling pathways to controlling the direction of migrating cells by measuring directionality (cos θ, Figure 5B) of HUVECs under three distinct conditions: point mutation to inhibit PLCγ (Y766F), treatment with a PI3K inhibitor (LY294002), and treatment with a MAPK inhibitor (PD0325901). Compared with the cos θ of HUVECs with only light stimulation, the directionality was decreased by Y766F mutation and LY294002 treatment, whereas PD0325902 treatment hardly induced any changes in directionality (Figure 5D). These results indicate that the PI3K and PLCγ pathways are actively involved in regulation of directionality, in which the PI3K pathway seems to have the most significant role ($p < 0.05$). Nevertheless, inhibition of any one of these pathways did not lead to a complete loss of cell directionality, as shown by cells expressing optoFGFR1 without light (– light) or expressing optoFGFR1 without CRY2PHR (ΔCRY2PHR). This implies that a complex and harmonized network among multiple signaling pathways is orchestrated to determine direction during cell migration (Ridley et al., 2003).

To identify the relationship of the motile properties during light-induced cell migration, we selected cells in which the total distance of migration was greater than 100 μm, which is the average length of a HUVEC. The overall distance from the center of the region of illumination (ROI) to the cells reduced constantly upon repeated light stimulation (Figure S5A), providing direct evidence of the phototactic movement of cells. Near the ROI where cells were partially illuminated, directionality toward the ROI increased without significantly affecting migration speed. However, when cells arrived inside the ROI (where they were illuminated entirely), their directionality decreased rapidly and, simultaneously, migration speed increased (Figures S5B and S5C). Collectively, these results confirm that the PI3K and PLCγ pathways are actively involved in determining the directionality of migrating HUVECs and that FGFR1 signaling differentially regulates the directionality and speed of migrating cells, depending on the pattern of activation (Figure S5E).

DISCUSSION

In this study, we generated an optogenetic protein, optoFGFR1, that enables the precise, rapid, and reversible activation of FGFR1 signaling pathways using blue light. In particular, with optoFGFR1 and fine-tuned light exposure, we were able to analyze temporal information of FGFR downstream pathways. Especially the activity of optoFGFR1 could be distinctly regulated because the kinetics and amplitude of the signal are mainly dependent on the modulation pattern of light.

Our experiments with optoFGFR1-transfected HUVECs also showed that light stimulation of subcellular regions led to the dissociation of actin fibers and induction of lamellipodia at the site of illumination, leading to a change in cell polarity (Figures 4B–4D). These phenomena seem to be related to local changes in the activities of Rho GTPases, such as Rac and RhoA, that are mainly associated with the PI3K pathway (Fera et al., 2004). Rho GTPases are reported to be involved in lamellipodial protrusion in the leading edge of migrating cells (Ridley et al., 1992; Wu et al., 2009) and in the disassembly of stress fibers, in which cofilin plays a major role in accelerating F-actin turnover (Delorme et al., 2007), which provides a simple explanation for our observation in active remodeling of stress fibers by local delivery of light. In addition, the increase in directionality induced by optoFGFR1 was dependent on the activity of the PI3K pathway. When cells arrived in the light-stimulated area, the directionality was lost, and the migration speed increased. This further suggests a central role of PI3K-Rho GTPases in light-induced cell migration because Rac is reported to be a switch that controls directional persistence and speed in cell migration (Pankov et al., 2005).

Our optoFGFR1-mediated phototaxis model revealed that FGFR signaling can differentially regulate the mode of cell migration, depending on the activation patterns (symmetric or asymmetric; Figure S5E). These findings provide insights into the debate about whether FGFR signals contribute to the directionality or speed (i.e., chemotaxis or chemokinesis) of migrating cells, a question that has been difficult to resolve by use of other migration assays (Barkefors et al., 2008). The Boyden chamber assay, scratch wound healing assay, under-agarose assay, and microfluidic devices are used frequently to study cell migration. However, these methods cannot provide detailed spatial and temporal data for a single cell because of their low sensitivity and efficiency (Kramer et al., 2013). On the other hand, our phototaxis model provides accurate information about individual migrating cells through time-lapse imaging, is highly efficient (Movie S3), and has potential for use in diverse cell types. In addition, compared with microfluidic devices, our phototaxis model is free of fluidic shear stress, and guidance cues can be produced in two or more dimensions with precise resolution.

There are optogenetic tools that regulate individual downstream growth factor signals, such as Ras/Erk, based on the interaction between phytochrome-PIF (Toettcher et al., 2013) and PI3K pathways using cryptochrome 2-CIB (Idevall-Hagren et al., 2012). Compared with these techniques, optoFGFR1 is a hierarchically different tool, modulating the initiation of signaling pathways. The activation of optoFGFR1 can regulate multiple signaling pathways at once, leading to feedback systems and crosstalk among signals, thereby reproducing a more physiologic state. This can be an efficient way to reveal the combinatorial effect in a biological context. As exemplified in experiments using the phototaxis model, introducing a point mutation or treating inhibitors could allow us to see the role of each downstream signaling pathway of FGFR in determining the directionality of migrating cells (Figure 5D).

OptoFGFR1 has a potential for use in many different biological systems. Along with improvements in optical technology, including wireless in vivo optical devices (Kim et al., 2013), optoFGFR1 has a potential for use in various experimental models

in which spatiotemporally precise control of FGFR activity is necessary. In addition, recent discoveries have expanded the scope of FGF biology from proliferative and migratory functions to regulation of metabolism and behavior through the endocrine system (Bookout et al., 2013; Potthoff et al., 2012), extending the possible biological application of optoFGFR1. OptoFGFR1 is a chimeric protein, and the CRY2PHR domain can function as an independent module. Therefore, our basic design can be generalized to build activating modules for other RTKs and receptor families.

In conclusion, we provide a tool for regulating specified FGFR activity by light, optoFGFR1, allowing studies of the function and downstream process of FGFR through spatiotemporal and precise control of its activity. OptoFGFR1 is a potentially powerful tool that can be used to elucidate FGFR signaling mechanisms in diverse aspects of biology.

SIGNIFICANCE

To date, various synthetic modules for the regulation of protein activity have been introduced to investigate the exact function of proteins and related signaling pathways. The optogenetic approach has been developed recently to regulate protein activity by introducing diverse photoactivatable modules represented by CRY2PHR from *Arabidopsis thaliana*. This optical approach has outstanding advantages, such as high spatiotemporal resolution, minimal side effects, and suitability for animal models. Here we provide an optogenetic regulatory module for FGFR signaling, optoFGFR1, in which blue light induces FGFR activation based on homointeraction of CRY2PHR. In this article, we showed that optoFGFR1 can regulate the signaling pathways of FGFR by blue light in a rapid and reversible manner with subcellular resolution. OptoFGFR1 also induces cell polarization, changes in the cytoskeleton, and directed cell migration by light illumination. Through migration experiments using optoFGFR1, we revealed that the PI3K and PLCγ pathways contribute differently to the directionality of endothelial cell migration and that FGFR signals affect both the directionality and speed of migrating cells. These results demonstrate that optoFGFR1 can be used to study numerous biological systems in which FGFR signals are involved, such as development, cancer, and angiogenesis. With growing interest regarding the role of FGFs, not only as typical growth factors but also as endocrine hormones, optoFGFR1 will be a valuable tool addressing needs in FGFR biology in vitro and in vivo.

EXPERIMENTAL PROCEDURES

Plasmids

For construction of optoFGFR1, the PHR domain from the CRY2PHR-mCherry vector (Kennedy et al., 2010) (provided by C. L. Tucker, University of Colorado Denver) was codon optimized (Lee et al., 2014), amplified by PCR, and inserted into the pmCitrine-N1 and pmCerulean-N1 vectors (Clontech). The cytoplasmic region of FGFR1 (amino acids 398–822) was isolated by RT-PCR with human brain total RNA (Clontech) and verified by sequencing. The myristoylation sequence was added to the N terminus of CRY2PHR, and the cytoplasmic region of FGFR1 was inserted between the myristoylation sequence and CRY2PHR using the In-Fusion cloning system (Clontech) according to the manufacturer's instructions. Site-directed mutation of Y766F in FGFR1 and D387A in CRY2PHR was done by multiple steps of PCR. The mCherry-Lifeact vector was constructed by inserting the Lifeact peptide sequence (Riedl et al., 2008) into the pmCherry-C1 vector (Clontech). The fluorescent protein sequence of yellow fluorescent protein (YFP)-PH_{AKT1} (Pleckstrin homology domain of AKT1) (Park et al., 2008; Yang et al., 2012) and ERK1-YFP (Alliance for Cellular Signaling) were replaced with dTomato from pThy1-Brainbow-1.0 L (Addgene, catalog no. 18725). Wild-type RAB5b was obtained from a small GTPase library (Heo and Meyer, 2003), cloned by PCR, and inserted into mRFP-C1. Chemically induced FGFR1 (ihFGFR1) was constructed based on the design of a previous study (Welm et al., 2002). In brief, the FK506 binding protein mutant (FKBP(36V)) in the pSH1/M-FGFR1-Fv-Fvls-E vector (Addgene, catalog no. 15285) was amplified by PCR, and the CRY2PHR region of optoFGFR1 plasmid was replaced with the two tandem repeats of FKBP(36V) using the In-Fusion cloning system. pCMV-R-GECO1 (catalog no. 32444) (Zhao et al., 2011) and pCMV-VSV-G (catalog no. 8454) were purchased from Addgene. The pLNCX2 vector was purchased from Clontech.

Cell Culture and Reagents

HeLa cells were cultured in Dulbecco's modified Eagle's medium (DMEM) (catalog no. 11995-065, Gibco) containing 10% fetal bovine serum (catalog no. 26140-079, Gibco) at 37°C with 10% CO_2. HUVECs (catalog no. C-003-5C, Gibco) were maintained in medium 200 (catalog no. M-200-500, Gibco) supplemented with 2% low-serum growth supplement (catalog no. S-003-10, Gibco) at 37°C with 5% CO_2. HUVECs between passages 5 and 9 were used for experiments. Transfection was conducted with the Neon transfection system (catalog no. MPK5000, Invitrogen) or Lipofectamine LTX (catalog no. 15338-100, Invitrogen) according to the manufacturer's instructions. In the case of HUVECs, the plate bottom was coated with 300 μg/ml of bovine collagen solution (PureCol, catalog no. 5005-B, Advanced BioMatrix) for 1 hr at 37°C before plating. Six hours before the experiments, serum starvation was performed with serum-free DMEM for HeLa cells or with human endothelial serum-free medium (catalog no. 11111-044, Gibco) containing 0.1% bovine serum albumin for HUVECs. A total of 10 ng/ml of bFGF (catalog no. 100-18B, PeproTech), 50 nM of PD0325901 (catalog no. 391210-10-9, Caymanchem), 50 μM of LY294002 (catalog no. L-7962, LC Laboratories), 20 μM of SU5402 (catalog no. 3300, Tocris), and 100 nM of AP20187 (catalog no. 635060, Clontech) was used for experiments. Inhibitors were added 30 min before the experiment.

Generation of a Stable Cell Line

BOSC 23 retroviral packaging cells (Pear et al., 1993) were plated onto a 60-mm dish 24 hr before transfection. Either the pLNCX2-R-GECO1 or pLNCX2-optoFGFR1 plasmid was transfected with pCMV-VSV-G into BOSC 23 cells (1:2 ratio) using Lipofectamine LTX following the manufacturer's instructions. After 48 hr, media containing retroviral particles were filtered through a 0.45-μm syringe filter (catalog no. 16555, Sartorius) and mixed with 8 μg/ml of Polybrene (catalog no. S2667, Sequa-brene, Sigma-Aldrich). The supernatant mixture was added to confluent HeLa cells in 100-mm dishes. Infected cells were transferred to 100-mm dishes at densities of 6×10^3 to 2.4×10^4 cells/dish and treated with 500 μg/ml of G418 (catalog no. G-1033, AG Scientific) for 2 weeks until clonal isolation.

Immunoblot Analysis

HeLa cells stably expressing optoFGFR1 were grown on 6-well plates and stimulated with an array of light-emitting diodes (LEDs) with 5.5 μW of 488 nm wavelength (Live Cell Instruments). Whole cell lysates were prepared in the dark room, harvested in ice-cold Dulbecco's phosphate-buffered saline (DPBS), and lysed with Pro-PREP solution (catalog no. 17081, iNtron Biotechnology). 30 μg of total protein was loaded onto a 4%–12% gradient polyacrylamide gel (catalog no. NP0322BOX, Invitrogen). After electrophoresis, proteins were transferred onto nitrocellulose membrane using the iBlot gel transfer device (catalog no. IB1001, Invitrogen). Membranes were stripped with BlotFresh Western blot stripping buffer (catalog no. SL100324, SignaGen Laboratories) before blotting with β-actin to remove signals from phospho-ERK1/2 and ERK1/2. Antibodies and related reagents used for immunoblot were phospho-FGFR1 Tyr653/654 (catalog no. 3476S, Cell Signaling

Technology), FGFR1 (catalog no. 9740S, Cell Signal), β-actin (catalog no. A5316, Sigma), phospho-ERK1/2 (catalog no. 9101S, Cell Signal), ERK1/2 (catalog no. 4696, Cell Signal), anti-mouse IR Dye 800CW (catalog no. 926-32210, LI-COR Biosciences), anti-rabbit IR Dye 600CW (catalog no. 926-68071, LI-COR Biosciences), and Odyssey blocking buffer (catalog no. 927-40000, LI-COR Biosciences). Protein bands were visualized using ODYSSEY CLx (catalog no. P/N 9140-WP, LI-COR Biosciences).

Live Cell Imaging and Photoactivation

Prepared cells were spread onto plastic-bottom, 96-well plates (catalog no. 89626, Ibidi) for live cell imaging. Live cell imaging was conducted with a Nikon A1R confocal microscope with CFI PlanApo objectives under 60× magnification for single cell imaging or 20× for monitoring cell migration. Lasers of 457 nm (cyan), 514 nm (yellow), and 561 nm (red) were used for acquisition of multicolor images. For FRET analysis, emission ratio imaging was performed with a 457-nm excitation laser/535-nm emission YFP HYQ filter (catalog no. 96345, Nikon).

Photoactivation was conducted with a 488-nm laser emitted through a Galvano scanner incorporated in a hybrid confocal scan head with a high-speed hyper selector (Nikon). The shape and size of the photoactivating region was adjusted by Nikon imaging software (NIS-element AR, Laboratory Imaging). The intensity of the activation laser was measured on the focus plane with an optical power meter (catalog no. 8230E, ADCMT). The activation intensity of the laser varied from 1–50 μW, which corresponds to 1.30–64.94 mW/cm^2.

A Nikon Ti-E TIRF microscope equipped with a CFI Apochromat TIRF 60× objective was used to specifically visualize plasma membrane fluorescence. The excitation light was produced from a directly doubled laser for GFP (488 nm) (CVI-Melles Griot). Emission filter fluorescein isothiocyanate (FITC) HYQ (catalog no. 96320, Nikon) was used for GFP, and an electron-multiplying charge-coupled device camera (catalog no. C9100-02, Hamamatsu Photonics) was used as a detector.

Image Analysis and Statistical Analysis

Image data were analyzed by Nikon imaging software (NIS-element AR, Laboratory Imaging) and MetaMorph 7.7 (Molecular Devices). Plotting intensity of ERK-dTomato, dTomato-PH$_{AKT}$, and R-GECO1 versus time (t) yielded a sigmoidal curve that was fitted to a four-parameter logistic function, generally expressed by the following equation (Dudley et al., 1985):

$$\text{Intensity}(t) = A + \frac{B - A}{1 + \left(\frac{t}{T_{1/2}}\right)^{-C}}, \qquad \text{(Equation 1)}$$

where A, B, C, and $T_{1/2}$ denote the minimum asymptote, maximum asymptote, steepness of curve, and inflection point, respectively. Nonlinear curve fitting was performed using the Solver tool in Microsoft Excel.

In the duty cycle experiment, we converted the duration of photostimulation into a duty cycle with the following equation, where T is the time period of stimulation and P is the total period of the signal:

$$\text{Duty cycle}(D) = \frac{T}{P} \times 100\ \%. \qquad \text{(Equation 2)}$$

MetaMorph 7.7 was used to quantify actin bundles in migrating HUVECs. To subtract noisy signals of the Lifeact biosensor, we used a binary operator in the software. A binarization process was applied to the original image to clearly visualize the linear actin pattern. The subtracted linear actin signals were measured and integrated into numerical values. Tracking of migrating cells was performed with a journal of multidimensional motion analysis in MetaMorph 7.7. Statistical comparisons were performed with an unpaired, two-tailed Student's t test using Microsoft Excel. SEM was used to indicate error bars in the figures.

Cell Viability Assay

OptoFGFR1 expressing or not expressing HeLa cells and HUVECs was plated on plastic-bottom, 96-well plates and illuminated by an LED array for 24 hr (488 nm, 25 μW, 5 min intervals). After light exposure, the cells were stained with LIVE/DEAD reagent (2 μM calcein-acetoxymethyl ester and 4 μM ethidium homodimer 1, catalog no. L-3224, Invitrogen) and incubated at 37°C for 30 min, followed by washing with DPBS. The images of stained cells were captured with Image Express XL (Molecular Devices). The number of live and dead cells was counted from four randomly selected fields for each condition. Cell viability was calculated as the percentage of the number of green fluorescence-stained cells of total cells.

SUPPLEMENTAL INFORMATION

Supplemental Information includes five figures and four movies and can be found with this article online at http://dx.doi.org/10.1016/j.chembiol.2014.05.013.

AUTHOR CONTRIBUTIONS

N.K. and W.D.H. conceived the idea, and W.D.H. directed the work. N.K., J.M.K., K.Y.C., and W.D.H. designed the experiments. N.K., J.M.K., M.L., and C.Y.K. performed the experiments. N.K., J.M.K., M.L., and K.Y.C. analyzed the data. N.K., J.M.K., M.L., C.Y.K., K.Y.C., and W.D.H. wrote the paper.

ACKNOWLEDGMENTS

We thank C.L. Tucker (University of Colorado) for CRY2PHR-mCherry. We also thank S. Lee and T. Kyung for critical discussions. This work was supported by National Creative Research Initiatives of MEST/NRF of Korea (2014001405) and by the KAIST Future Systems Healthcare Project from the Ministry of Science, ICT, and Future Planning.

Received: March 14, 2014
Revised: May 9, 2014
Accepted: May 27, 2014
Published: June 26, 2014

REFERENCES

Barkefors, I., Le Jan, S., Jakobsson, L., Hejll, E., Carlson, G., Johansson, H., Jarvius, J., Park, J.W., Li Jeon, N., and Kreuger, J. (2008). Endothelial cell migration in stable gradients of vascular endothelial growth factor A and fibroblast growth factor 2: effects on chemotaxis and chemokinesis. J. Biol. Chem. *283*, 13905–13912.

Bastaki, M., Nelli, E.E., Dell'Era, P., Rusnati, M., Molinari-Tosatti, M.P., Parolini, S., Auerbach, R., Ruco, L.P., Possati, L., and Presta, M. (1997). Basic fibroblast growth factor-induced angiogenic phenotype in mouse endothelium. A study of aortic and microvascular endothelial cell lines. Arterioscler. Thromb. Vasc. Biol. *17*, 454–464.

Bookout, A.L., de Groot, M.H.M., Owen, B.M., Lee, S., Gautron, L., Lawrence, H.L., Ding, X., Elmquist, J.K., Takahashi, J.S., Mangelsdorf, D.J., and Kliewer, S.A. (2013). FGF21 regulates metabolism and circadian behavior by acting on the nervous system. Nat. Med. *19*, 1147–1152.

Bugaj, L.J., Choksi, A.T., Mesuda, C.K., Kane, R.S., and Schaffer, D.V. (2013). Optogenetic protein clustering and signaling activation in mammalian cells. Nat. Methods *10*, 249–252.

Delorme, V., Machacek, M., DerMardirossian, C., Anderson, K.L., Wittmann, T., Hanein, D., Waterman-Storer, C., Danuser, G., and Bokoch, G.M. (2007). Cofilin activity downstream of Pak1 regulates cell protrusion efficiency by organizing lamellipodium and lamella actin networks. Dev. Cell *13*, 646–662.

Dudley, R.A., Edwards, P., Ekins, R.P., Finney, D.J., McKenzie, I.G., Raab, G.M., Rodbard, D., and Rodgers, R.P. (1985). Guidelines for immunoassay data processing. Clin. Chem. *31*, 1264–1271.

Fera, E., O'Neil, C., Lee, W., Li, S., and Pickering, J.G. (2004). Fibroblast growth factor-2 and remodeled type I collagen control membrane protrusion in human vascular smooth muscle cells: biphasic activation of Rac1. J. Biol. Chem. *279*, 35573–35582.

Freeman, K.W., Gangula, R.D., Welm, B.E., Ozen, M., Foster, B.A., Rosen, J.M., Ittmann, M., Greenberg, N.M., and Spencer, D.M. (2003). Conditional activation of fibroblast growth factor receptor (FGFR) 1, but not FGFR2, in prostate cancer cells leads to increased osteopontin induction, extracellular

signal-regulated kinase activation, and in vivo proliferation. Cancer Res. *63*, 6237–6243.

Heo, W.D., and Meyer, T. (2003). Switch-of-function mutants based on morphology classification of Ras superfamily small GTPases. Cell *113*, 315–328.

Hubbard, S.R., and Till, J.H. (2000). Protein tyrosine kinase structure and function. Annu. Rev. Biochem. *69*, 373–398.

Idevall-Hagren, O., Dickson, E.J., Hille, B., Toomre, D.K., and De Camilli, P. (2012). Optogenetic control of phosphoinositide metabolism. Proc. Natl. Acad. Sci. USA *109*, E2316–E2323.

Itoh, N., and Ornitz, D.M. (2004). Evolution of the Fgf and Fgfr gene families. Trends Genet. *20*, 563–569.

Kennedy, M.J., Hughes, R.M., Peteya, L.A., Schwartz, J.W., Ehlers, M.D., and Tucker, C.L. (2010). Rapid blue-light-mediated induction of protein interactions in living cells. Nat. Methods *7*, 973–975.

Kim, T.I., McCall, J.G., Jung, Y.H., Huang, X., Siuda, E.R., Li, Y., Song, J., Song, Y.M., Pao, H.A., Kim, R.-H., et al. (2013). Injectable, cellular-scale optoelectronics with applications for wireless optogenetics. Science *340*, 211–216.

Klint, P., and Claesson-Welsh, L. (1999). Signal transduction by fibroblast growth factor receptors. Front. Biosci. *4*, D165–D177.

Kramer, N., Walzl, A., Unger, C., Rosner, M., Krupitza, G., Hengstschläger, M., and Dolznig, H. (2013). In vitro cell migration and invasion assays. Mutat. Res. *752*, 10–24.

Lamalice, L., Le Boeuf, F., and Huot, J. (2007). Endothelial cell migration during angiogenesis. Circ. Res. *100*, 782–794.

Lee, S., Park, H., Kyung, T., Kim, N.Y., Kim, S., Kim, J., and Heo, W.D. (2014). Reversible protein inactivation by optogenetic trapping in cells. Nat. Methods *11*, 633–636.

Levskaya, A., Weiner, O.D., Lim, W.A., and Voigt, C.A. (2009). Spatiotemporal control of cell signalling using a light-switchable protein interaction. Nature *461*, 997–1001.

Liu, H., Yu, X., Li, K., Klejnot, J., Yang, H., Lisiero, D., and Lin, C. (2008). Photoexcited CRY2 interacts with CIB1 to regulate transcription and floral initiation in Arabidopsis. Science *322*, 1535–1539.

Marshall, C.J. (1995). Specificity of receptor tyrosine kinase signaling: transient versus sustained extracellular signal-regulated kinase activation. Cell *80*, 179–185.

Mohammadi, M., Honegger, A.M., Rotin, D., Fischer, R., Bellot, F., Li, W., Dionne, C.A., Jaye, M., Rubinstein, M., and Schlessinger, J. (1991). A tyrosine-phosphorylated carboxy-terminal peptide of the fibroblast growth factor receptor (Flg) is a binding site for the SH2 domain of phospholipase C-gamma 1. Mol. Cell. Biol. *11*, 5068–5078.

Mohammadi, M., Dikic, I., Sorokin, A., Burgess, W.H., Jaye, M., and Schlessinger, J. (1996). Identification of six novel autophosphorylation sites on fibroblast growth factor receptor 1 and elucidation of their importance in receptor activation and signal transduction. Mol. Cell. Biol. *16*, 977–989.

Neff, T., and Blau, C.A. (2001). Pharmacologically regulated cell therapy. Blood *97*, 2535–2540.

Pankov, R., Endo, Y., Even-Ram, S., Araki, M., Clark, K., Cukierman, E., Matsumoto, K., and Yamada, K.M. (2005). A Rac switch regulates random versus directionally persistent cell migration. J. Cell Biol. *170*, 793–802.

Park, W.S., Heo, W.D., Whalen, J.H., O'Rourke, N.A., Bryan, H.M., Meyer, T., and Teruel, M.N. (2008). Comprehensive identification of PIP3-regulated PH domains from C. elegans to H. sapiens by model prediction and live imaging. Mol. Cell *30*, 381–392.

Pear, W.S., Nolan, G.P., Scott, M.L., and Baltimore, D. (1993). Production of high-titer helper-free retroviruses by transient transfection. Proc. Natl. Acad. Sci. USA *90*, 8392–8396.

Potthoff, M.J., Kliewer, S.A., and Mangelsdorf, D.J. (2012). Endocrine fibroblast growth factors 15/19 and 21: from feast to famine. Genes Dev. *26*, 312–324.

Powers, C.J., McLeskey, S.W., and Wellstein, A. (2000). Fibroblast growth factors, their receptors and signaling. Endocr. Relat. Cancer *7*, 165–197.

Ridley, A.J., Paterson, H.F., Johnston, C.L., Diekmann, D., and Hall, A. (1992). The small GTP-binding protein rac regulates growth factor-induced membrane ruffling. Cell *70*, 401–410.

Ridley, A.J., Schwartz, M.A., Burridge, K., Firtel, R.A., Ginsberg, M.H., Borisy, G., Parsons, J.T., and Horwitz, A.R. (2003). Cell migration: integrating signals from front to back. Science *302*, 1704–1709.

Riedl, J., Crevenna, A.H., Kessenbrock, K., Yu, J.H., Neukirchen, D., Bista, M., Bradke, F., Jenne, D., Holak, T.A., Werb, Z., et al. (2008). Lifeact: a versatile marker to visualize F-actin. Nat. Methods *5*, 605–607.

Sandilands, E., Akbarzadeh, S., Vecchione, A., McEwan, D.G., Frame, M.C., and Heath, J.K. (2007). Src kinase modulates the activation, transport and signalling dynamics of fibroblast growth factor receptors. EMBO Rep. *8*, 1162–1169.

Shi, C., Lu, J., Wu, W., Ma, F., Georges, J., Huang, H., Balducci, J., Chang, Y., and Huang, Y. (2011). Endothelial cell-specific molecule 2 (ECSM2) localizes to cell-cell junctions and modulates bFGF-directed cell migration via the ERK-FAK pathway. PLoS ONE *6*, e21482.

Stockwell, B.R. (2000). Chemical genetics: ligand-based discovery of gene function. Nat. Rev. Genet. *1*, 116–125.

Taylor, C.W. (1998). Inositol trisphosphate receptors: Ca^{2+}-modulated intracellular Ca^{2+} channels. Biochim. Biophys. Acta *1436*, 19–33.

Tkachenko, E., Sabouri-Ghomi, M., Pertz, O., Kim, C., Gutierrez, E., Machacek, M., Groisman, A., Danuser, G., and Ginsberg, M.H. (2011). Protein kinase A governs a RhoA-RhoGDI protrusion-retraction pacemaker in migrating cells. Nat. Cell Biol. *13*, 660–667.

Toettcher, J.E., Weiner, O.D., and Lim, W.A. (2013). Using optogenetics to interrogate the dynamic control of signal transmission by the Ras/Erk module. Cell *155*, 1422–1434.

Tsai, F.-C., Seki, A., Yang, H.W., Hayer, A., Carrasco, S., Malmersjö, S., and Meyer, T. (2014). A polarized Ca^{2+}, diacylglycerol and STIM1 signalling system regulates directed cell migration. Nat. Cell Biol. *16*, 133–144.

Turner, N., and Grose, R. (2010). Fibroblast growth factor signalling: from development to cancer. Nat. Rev. Cancer *10*, 116–129.

Welf, E.S., Ahmed, S., Johnson, H.E., Melvin, A.T., and Haugh, J.M. (2012). Migrating fibroblasts reorient directionality by a metastable, PI3K-dependent mechanism. J. Cell Biol. *197*, 105–114.

Welm, B.E., Freeman, K.W., Chen, M., Contreras, A., Spencer, D.M., and Rosen, J.M. (2002). Inducible dimerization of FGFR1: development of a mouse model to analyze progressive transformation of the mammary gland. J. Cell Biol. *157*, 703–714.

Wiley, H.S., and Burke, P.M. (2001). Regulation of receptor tyrosine kinase signaling by endocytic trafficking. Traffic *2*, 12–18.

Wong, A., Lamothe, B., Lee, A., Schlessinger, J., and Lax, I. (2002). FRS2 alpha attenuates FGF receptor signaling by Grb2-mediated recruitment of the ubiquitin ligase Cbl. Proc. Natl. Acad. Sci. USA *99*, 6684–6689.

Wu, Y.I., Frey, D., Lungu, O.I., Jaehrig, A., Schlichting, I., Kuhlman, B., and Hahn, K.M. (2009). A genetically encoded photoactivatable Rac controls the motility of living cells. Nature *461*, 104–108.

Xian, W., Schwertfeger, K.L., Vargo-Gogola, T., and Rosen, J.M. (2005). Pleiotropic effects of FGFR1 on cell proliferation, survival, and migration in a 3D mammary epithelial cell model. J. Cell Biol. *171*, 663–673.

Yang, H.W., Shin, M.-G., Lee, S., Kim, J.-R., Park, W.S., Cho, K.-H., Meyer, T., and Heo, W.D. (2012). Cooperative activation of PI3K by Ras and Rho family small GTPases. Mol. Cell *47*, 281–290.

Yu, X., Sayegh, R., Maymon, M., Warpeha, K., Klejnot, J., Yang, H., Huang, J., Lee, J., Kaufman, L., and Lin, C. (2009). Formation of nuclear bodies of Arabidopsis CRY2 in response to blue light is associated with its blue light-dependent degradation. Plant Cell *21*, 118–130.

Zhao, Y., Araki, S., Wu, J., Teramoto, T., Chang, Y.-F., Nakano, M., Abdelfattah, A.S., Fujiwara, M., Ishihara, T., Nagai, T., and Campbell, R.E. (2011). An expanded palette of genetically encoded Ca^{2+} indicators. Science *333*, 1888–1891.